

MIT Open Access Articles

Measurement of D^0 - \bar{D}^0 mixing and CP violation in two-body D^0 decays

The MIT Faculty has made this article openly available. **Please share** how this access benefits you. Your story matters.

Citation: Lees, J. P. et al. "Measurement of D^0 - \bar{D}^0 Mixing and CP Violation in Two-body D^0 Decays." Physical Review D 87.1 (2013). © 2013 American Physical Society

As Published: <http://dx.doi.org/10.1103/PhysRevD.87.012004>

Publisher: American Physical Society

Persistent URL: <http://hdl.handle.net/1721.1/77141>

Version: Final published version: final published article, as it appeared in a journal, conference proceedings, or other formally published context

Terms of Use: Article is made available in accordance with the publisher's policy and may be subject to US copyright law. Please refer to the publisher's site for terms of use.



Measurement of D^0 - \bar{D}^0 mixing and CP violation in two-body D^0 decays

J. P. Lees,¹ V. Poireau,¹ V. Tisserand,¹ J. Garra Tico,² E. Grauges,² A. Palano,^{3a,3b} G. Eigen,⁴ B. Stugu,⁴ D. N. Brown,⁵ L. T. Kerth,⁵ Yu. G. Kolomensky,⁵ G. Lynch,⁵ H. Koch,⁶ T. Schroeder,⁶ D. J. Asgeirsson,⁷ C. Hearty,⁷ T. S. Mattison,⁷ J. A. McKenna,⁷ R. Y. So,⁷ A. Khan,⁸ V. E. Blinov,⁹ A. R. Buzykaev,⁹ V. P. Druzhinin,⁹ V. B. Golubev,⁹ E. A. Kravchenko,⁹ A. P. Onuchin,⁹ S. I. Serednyakov,⁹ Yu. I. Skovpen,⁹ E. P. Solodov,⁹ K. Yu. Todyshev,⁹ A. N. Yushkov,⁹ M. Bondioli,¹⁰ D. Kirkby,¹⁰ A. J. Lankford,¹⁰ M. Mandelkern,¹⁰ H. Atmacan,¹¹ J. W. Gary,¹¹ F. Liu,¹¹ O. Long,¹¹ G. M. Vitug,¹¹ C. Campagnari,¹² T. M. Hong,¹² D. Kovalskyi,¹² J. D. Richman,¹² C. A. West,¹² A. M. Eisner,¹³ J. Kroseberg,¹³ W. S. Lockman,¹³ A. J. Martinez,¹³ B. A. Schumm,¹³ A. Seiden,¹³ D. S. Chao,¹⁴ C. H. Cheng,¹⁴ B. Echenard,¹⁴ K. T. Flood,¹⁴ D. G. Hitlin,¹⁴ P. Ongmongkolkul,¹⁴ F. C. Porter,¹⁴ A. Y. Rakitin,¹⁴ R. Andreassen,¹⁵ Z. Huard,¹⁵ B. T. Meadows,¹⁵ M. D. Sokoloff,¹⁵ L. Sun,¹⁵ P. C. Bloom,¹⁶ W. T. Ford,¹⁶ A. Gaz,¹⁶ U. Nauenberg,¹⁶ J. G. Smith,¹⁶ S. R. Wagner,¹⁶ R. Ayad,^{17,*} W. H. Toki,¹⁷ B. Spaan,¹⁸ K. R. Schubert,¹⁹ R. Schwierz,¹⁹ D. Bernard,²⁰ M. Verderi,²⁰ P. J. Clark,²¹ S. Playfer,²¹ D. Bettoni,^{22a} C. Bozzi,^{22a} R. Calabrese,^{22a,22b} G. Cibinetto,^{22a,22b} E. Fioravanti,^{22a,22b} I. Garzia,^{22a,22b} E. Luppi,^{22a,22b} M. Munerato,^{22a,22b} L. Piemontese,^{22a} V. Santoro,^{22a} R. Baldini-Ferroli,²³ A. Calcaterra,²³ R. de Sangro,²³ G. Finocchiaro,²³ P. Patteri,²³ I. M. Peruzzi,^{23,†} M. Piccolo,²³ M. Rama,²³ A. Zallo,²³ R. Contri,^{24a,24b} E. Guido,^{24a,24b} M. Lo Vetere,^{24a,24b} M. R. Monge,^{24a,24b} S. Passaggio,^{24a} C. Patrignani,^{24a,24b} E. Robutti,^{24a} B. Bhuyan,²⁵ V. Prasad,²⁵ C. L. Lee,²⁶ M. Morii,²⁶ A. J. Edwards,²⁷ A. Adametz,²⁸ U. Uwer,²⁸ H. M. Lacker,²⁹ T. Lueck,²⁹ P. D. Dauncey,³⁰ U. Mallik,³¹ C. Chen,³² J. Cochran,³² W. T. Meyer,³² S. Prell,³² A. E. Rubin,³² A. V. Gritsan,³³ Z. J. Guo,³³ N. Arnaud,³⁴ M. Davier,³⁴ D. Derkach,³⁴ G. Grosdidier,³⁴ F. Le Diberder,³⁴ A. M. Lutz,³⁴ B. Malaescu,³⁴ P. Roudeau,³⁴ M. H. Schune,³⁴ A. Stocchi,³⁴ G. Wormser,³⁴ D. J. Lange,³⁵ D. M. Wright,³⁵ C. A. Chavez,³⁶ J. P. Coleman,³⁶ J. R. Fry,³⁶ E. Gabathuler,³⁶ D. E. Hutchcroft,³⁶ D. J. Payne,³⁶ C. Touramanis,³⁶ A. J. Bevan,³⁷ F. Di Lodovico,³⁷ R. Sacco,³⁷ M. Sigamani,³⁷ G. Cowan,³⁸ D. N. Brown,³⁹ C. L. Davis,³⁹ A. G. Denig,⁴⁰ M. Fritsch,⁴⁰ W. Gradl,⁴⁰ K. Griessinger,⁴⁰ A. Hafner,⁴⁰ E. Prencipe,⁴⁰ R. J. Barlow,^{41,‡} G. Jackson,⁴¹ G. D. Lafferty,⁴¹ E. Behn,⁴² R. Cenci,⁴² B. Hamilton,⁴² A. Jawahery,⁴² D. A. Roberts,⁴² C. Dallapiccola,⁴³ R. Cowan,⁴⁴ D. Dujmic,⁴⁴ G. Sciolla,⁴⁴ R. Cheaib,⁴⁵ D. Lindemann,⁴⁵ P. M. Patel,^{45,§} S. H. Robertson,⁴⁵ P. Biassoni,^{46a,46b} N. Neri,^{46a} F. Palombo,^{46a,46b} S. Stracka,^{46a,46b} L. Cremaldi,⁴⁷ R. Godang,^{47,||} R. Kroeger,⁴⁷ P. Sonnek,⁴⁷ D. J. Summers,⁴⁷ X. Nguyen,⁴⁸ M. Simard,⁴⁸ P. Taras,⁴⁸ G. De Nardo,^{49a,49b} D. Monorchio,^{49a,49b} G. Onorato,^{49a,49b} C. Sciacca,^{49a,49b} M. Martinelli,⁵⁰ G. Raven,⁵⁰ C. P. Jessop,⁵¹ J. M. LoSecco,⁵¹ W. F. Wang,⁵¹ K. Honscheid,⁵² R. Kass,⁵² J. Brau,⁵³ R. Frey,⁵³ N. B. Sinev,⁵³ D. Strom,⁵³ E. Torrence,⁵³ E. Feltresi,^{54a,54b} N. Gagliardi,^{54a,54b} M. Margoni,^{54a,54b} M. Morandin,^{54a} M. Posocco,^{54a} M. Rotondo,^{54a} G. Simi,^{54a} F. Simonetto,^{54a,54b} R. Stroili,^{54a,54b} S. Akar,⁵⁵ E. Ben-Haim,⁵⁵ M. Bomben,⁵⁵ G. R. Bonneaud,⁵⁵ H. Briand,⁵⁵ G. Calderini,⁵⁵ J. Chauveau,⁵⁵ O. Hamon,⁵⁵ Ph. Leruste,⁵⁵ G. Marchiori,⁵⁵ J. Ocariz,⁵⁵ S. Sitt,⁵⁵ M. Biasini,^{56a,56b} E. Manoni,^{56a,56b} S. Pacetti,^{56a,56b} A. Rossi,^{56a,56b} C. Angelini,^{57a,57b} G. Batignani,^{57a,57b} S. Bettarini,^{57a,57b} M. Carpinelli,^{57a,57b,¶} G. Casarosa,^{57a,57b} A. Cervelli,^{57a,57b} F. Forti,^{57a,57b} M. A. Giorgi,^{57a,57b} A. Lusiani,^{57a,57c} B. Oberhof,^{57a,57b} E. Paoloni,^{57a,57b} A. Perez,^{57a} G. Rizzo,^{57a,57b} J. J. Walsh,^{57a} D. Lopes Pegna,⁵⁸ J. Olsen,⁵⁸ A. J. S. Smith,⁵⁸ A. V. Telnov,⁵⁸ F. Anulli,^{59a} R. Faccini,^{59a,59b} F. Ferrarotto,^{59a} F. Ferroni,^{59a,59b} M. Gaspero,^{59a,59b} L. Li Gioi,^{59a} M. A. Mazzoni,^{59a} G. Piredda,^{59a} C. Büniger,⁶⁰ O. Grünberg,⁶⁰ T. Hartmann,⁶⁰ T. Leddig,⁶⁰ H. Schröder,^{60,§} C. Voss,⁶⁰ R. Waldi,⁶⁰ T. Adye,⁶¹ E. O. Olaiya,⁶¹ F. F. Wilson,⁶¹ S. Emery,⁶² G. Hamel de Monchenault,⁶² G. Vasseur,⁶² Ch. Yèche,⁶² D. Aston,⁶³ D. J. Bard,⁶³ R. Bartoldus,⁶³ J. F. Benitez,⁶³ C. Cartaro,⁶³ M. R. Convery,⁶³ J. Dorfan,⁶³ G. P. Dubois-Felsmann,⁶³ W. Dunwoodie,⁶³ M. Ebert,⁶³ R. C. Field,⁶³ M. Franco Sevilla,⁶³ B. G. Fulsom,⁶³ A. M. Gabareen,⁶³ M. T. Graham,⁶³ P. Grenier,⁶³ C. Hast,⁶³ W. R. Innes,⁶³ M. H. Kelsey,⁶³ P. Kim,⁶³ M. L. Kocian,⁶³ D. W. G. S. Leith,⁶³ P. Lewis,⁶³ B. Lindquist,⁶³ S. Luitz,⁶³ V. Luth,⁶³ H. L. Lynch,⁶³ D. B. MacFarlane,⁶³ D. R. Muller,⁶³ H. Neal,⁶³ S. Nelson,⁶³ M. Perl,⁶³ T. Pulliam,⁶³ B. N. Ratcliff,⁶³ A. Roodman,⁶³ A. A. Salnikov,⁶³ R. H. Schindler,⁶³ A. Snyder,⁶³ D. Su,⁶³ M. K. Sullivan,⁶³ J. Va'vra,⁶³ A. P. Wagner,⁶³ W. J. Wisniewski,⁶³ M. Wittgen,⁶³ D. H. Wright,⁶³ H. W. Wulsin,⁶³ C. C. Young,⁶³ V. Ziegler,⁶³ W. Park,⁶⁴ M. V. Purohit,⁶⁴ R. M. White,⁶⁴ J. R. Wilson,⁶⁴ A. Randle-Conde,⁶⁵ S. J. Sekula,⁶⁵ M. Bellis,⁶⁶ P. R. Burchat,⁶⁶ T. S. Miyashita,⁶⁶ E. M. T. Puccio,⁶⁶ M. S. Alam,⁶⁷ J. A. Ernst,⁶⁷ R. Gorodeisky,⁶⁸ N. Guttman,⁶⁸ D. R. Peimer,⁶⁸ A. Soffer,⁶⁸ P. Lund,⁶⁹ S. M. Spanier,⁶⁹ J. L. Ritchie,⁷⁰ A. M. Ruland,⁷⁰ R. F. Schwitters,⁷⁰ B. C. Wray,⁷⁰ J. M. Izen,⁷¹ X. C. Lou,⁷¹ F. Bianchi,^{72a,72b} D. Gamba,^{72a,72b} S. Zambito,^{72a,72b} L. Lancieri,^{73a,73b} L. Vitale,^{73a,73b} F. Martinez-Vidal,⁷⁴ A. Oyanguren,⁷⁴ H. Ahmed,⁷⁵ J. Albert,⁷⁵ Sw. Banerjee,⁷⁵ F. U. Bernlochner,⁷⁵ H. H. F. Choi,⁷⁵ G. J. King,⁷⁵ R. Kowalewski,⁷⁵ M. J. Lewczuk,⁷⁵ I. M. Nugent,⁷⁵ J. M. Roney,⁷⁵ R. J. Sobie,⁷⁵ N. Tasneem,⁷⁵ T. J. Gershon,⁷⁶ P. F. Harrison,⁷⁶ T. E. Latham,⁷⁶ H. R. Band,⁷⁷ S. Dasu,⁷⁷ Y. Pan,⁷⁷ R. Prepost,⁷⁷ and S. L. Wu⁷⁷

(BABAR Collaboration)

- ¹Laboratoire d'Annecy-le-Vieux de Physique des Particules (LAPP), Université de Savoie, CNRS/IN2P3, F-74941 Annecy-Le-Vieux, France
- ²Departament ECM, Universitat de Barcelona, Facultat de Física, E-08028 Barcelona, Spain
- ^{3a}INFN Sezione di Bari, I-70126 Bari, Italy
- ^{3b}Dipartimento di Fisica, Università di Bari, I-70126 Bari, Italy
- ⁴University of Bergen, Institute of Physics, N-5007 Bergen, Norway
- ⁵Lawrence Berkeley National Laboratory and University of California, Berkeley, California 94720, USA
- ⁶Ruhr Universität Bochum, Institut für Experimentalphysik 1, D-44780 Bochum, Germany
- ⁷University of British Columbia, Vancouver, British Columbia, Canada V6T 1Z1
- ⁸Brunel University, Uxbridge, Middlesex UB8 3PH, United Kingdom
- ⁹Budker Institute of Nuclear Physics, Novosibirsk 630090, Russia
- ¹⁰University of California at Irvine, Irvine, California 92697, USA
- ¹¹University of California at Riverside, Riverside, California 92521, USA
- ¹²University of California at Santa Barbara, Santa Barbara, California 93106, USA
- ¹³University of California at Santa Cruz, Institute for Particle Physics, Santa Cruz, California 95064, USA
- ¹⁴California Institute of Technology, Pasadena, California 91125, USA
- ¹⁵University of Cincinnati, Cincinnati, Ohio 45221, USA
- ¹⁶University of Colorado, Boulder, Colorado 80309, USA
- ¹⁷Colorado State University, Fort Collins, Colorado 80523, USA
- ¹⁸Technische Universität Dortmund, Fakultät Physik, D-44221 Dortmund, Germany
- ¹⁹Technische Universität Dresden, Institut für Kern- und Teilchenphysik, D-01062 Dresden, Germany
- ²⁰Laboratoire Leprince-Ringuet, Ecole Polytechnique, CNRS/IN2P3, F-91128 Palaiseau, France
- ²¹University of Edinburgh, Edinburgh EH9 3JZ, United Kingdom
- ^{22a}INFN Sezione di Ferrara, I-44100 Ferrara, Italy
- ^{22b}Dipartimento di Fisica, Università di Ferrara, I-44100 Ferrara, Italy
- ²³INFN Laboratori Nazionali di Frascati, I-00044 Frascati, Italy
- ^{24a}INFN Sezione di Genova, I-16146 Genova, Italy
- ^{24b}Dipartimento di Fisica, Università di Genova, I-16146 Genova, Italy
- ²⁵Indian Institute of Technology Guwahati, Guwahati, Assam, 781 039, India
- ²⁶Harvard University, Cambridge, Massachusetts 02138, USA
- ²⁷Harvey Mudd College, Claremont, California 91711, USA
- ²⁸Universität Heidelberg, Physikalisches Institut, Philosophenweg 12, D-69120 Heidelberg, Germany
- ²⁹Humboldt-Universität zu Berlin, Institut für Physik, Newtonstr. 15, D-12489 Berlin, Germany
- ³⁰Imperial College London, London, SW7 2AZ, United Kingdom
- ³¹University of Iowa, Iowa City, Iowa 52242, USA
- ³²Iowa State University, Ames, Iowa 50011-3160, USA
- ³³Johns Hopkins University, Baltimore, Maryland 21218, USA
- ³⁴Laboratoire de l'Accélérateur Linéaire, IN2P3/CNRS et Université Paris-Sud 11, Centre Scientifique d'Orsay, B. P. 34, F-91898 Orsay Cedex, France
- ³⁵Lawrence Livermore National Laboratory, Livermore, California 94550, USA
- ³⁶University of Liverpool, Liverpool L69 7ZE, United Kingdom
- ³⁷Queen Mary, University of London, London, E1 4NS, United Kingdom
- ³⁸University of London, Royal Holloway and Bedford New College, Egham, Surrey TW20 0EX, United Kingdom
- ³⁹University of Louisville, Louisville, Kentucky 40292, USA
- ⁴⁰Johannes Gutenberg-Universität Mainz, Institut für Kernphysik, D-55099 Mainz, Germany
- ⁴¹University of Manchester, Manchester M13 9PL, United Kingdom
- ⁴²University of Maryland, College Park, Maryland 20742, USA
- ⁴³University of Massachusetts, Amherst, Massachusetts 01003, USA
- ⁴⁴Laboratory for Nuclear Science, Massachusetts Institute of Technology, Cambridge, Massachusetts 02139, USA
- ⁴⁵McGill University, Montréal, Québec, Canada H3A 2T8
- ^{46a}INFN Sezione di Milano, I-20133 Milano, Italy
- ^{46b}Dipartimento di Fisica, Università di Milano, I-20133 Milano, Italy
- ⁴⁷University of Mississippi, University, Mississippi 38677, USA
- ⁴⁸Université de Montréal, Physique des Particules, Montréal, Québec, Canada H3C 3J7
- ^{49a}INFN Sezione di Napoli, I-80126 Napoli, Italy
- ^{49b}Dipartimento di Scienze Fisiche, Università di Napoli Federico II, I-80126 Napoli, Italy
- ⁵⁰NIKHEF, National Institute for Nuclear Physics and High Energy Physics, NL-1009 DB Amsterdam, Netherlands

- ⁵¹University of Notre Dame, Notre Dame, Indiana 46556, USA
⁵²Ohio State University, Columbus, Ohio 43210, USA
⁵³University of Oregon, Eugene, Oregon 97403, USA
^{54a}INFN Sezione di Padova, I-35131 Padova, Italy
^{54b}Dipartimento di Fisica, Università di Padova, I-35131 Padova, Italy
⁵⁵Laboratoire de Physique Nucléaire et de Hautes Energies, IN2P3/CNRS, Université Pierre et Marie Curie-Paris6, Université Denis Diderot-Paris7, F-75252 Paris, France
^{56a}INFN Sezione di Perugia, I-06100 Perugia, Italy
^{56b}Dipartimento di Fisica, Università di Perugia, I-06100 Perugia, Italy
^{57a}INFN Sezione di Pisa, I-56127 Pisa, Italy
^{57b}Dipartimento di Fisica, Università di Pisa, I-56127 Pisa, Italy
^{57c}Scuola Normale Superiore di Pisa, I-56127 Pisa, Italy
⁵⁸Princeton University, Princeton, New Jersey 08544, USA
^{59a}INFN Sezione di Roma, I-00185 Roma, Italy
^{59b}Dipartimento di Fisica, Università di Roma La Sapienza, I-00185 Roma, Italy
⁶⁰Universität Rostock, D-18051 Rostock, Germany
⁶¹Rutherford Appleton Laboratory, Chilton, Didcot, Oxon, OX11 0QX, United Kingdom
⁶²CEA, Irfu, SPP, Centre de Saclay, F-91191 Gif-sur-Yvette, France
⁶³SLAC National Accelerator Laboratory, Stanford, California 94309, USA
⁶⁴University of South Carolina, Columbia, South Carolina 29208, USA
⁶⁵Southern Methodist University, Dallas, Texas 75275, USA
⁶⁶Stanford University, Stanford, California 94305-4060, USA
⁶⁷State University of New York, Albany, New York 12222, USA
⁶⁸Tel Aviv University, School of Physics and Astronomy, Tel Aviv, 69978, Israel
⁶⁹University of Tennessee, Knoxville, Tennessee 37996, USA
⁷⁰University of Texas at Austin, Austin, Texas 78712, USA
⁷¹University of Texas at Dallas, Richardson, Texas 75083, USA
^{72a}INFN Sezione di Torino, I-10125 Torino, Italy
^{72b}Dipartimento di Fisica Sperimentale, Università di Torino, I-10125 Torino, Italy
^{73a}INFN Sezione di Trieste, I-34127 Trieste, Italy
^{73b}Dipartimento di Fisica, Università di Trieste, I-34127 Trieste, Italy
⁷⁴IFIC, Universitat de Valencia-CSIC, E-46071 Valencia, Spain
⁷⁵University of Victoria, Victoria, British Columbia, Canada V8W 3P6
⁷⁶Department of Physics, University of Warwick, Coventry CV4 7AL, United Kingdom
⁷⁷University of Wisconsin, Madison, Wisconsin 53706, USA
(Received 20 September 2012; published 3 January 2013)

We present a measurement of D^0 - \bar{D}^0 mixing and CP violation using the ratio of lifetimes simultaneously extracted from a sample of D^0 mesons produced through the flavor-tagged process $D^{*+} \rightarrow D^0 \pi^+$, where D^0 decays to $K^+ \pi^-$, $K^- K^+$, or $\pi^- \pi^+$, along with the untagged decays $D^0 \rightarrow K^+ \pi^-$ and $D^0 \rightarrow K^- K^+$. The lifetimes of the CP -even, Cabibbo-suppressed modes $K^- K^+$ and $\pi^- \pi^+$ are compared to that of the CP -mixed mode $K^+ \pi^-$ in order to measure y_{CP} and ΔY . We obtain $y_{CP} = [0.72 \pm 0.18(\text{stat}) \pm 0.12(\text{syst})]\%$ and $\Delta Y = [0.09 \pm 0.26(\text{stat}) \pm 0.06(\text{syst})]\%$, where ΔY constrains possible CP violation. The y_{CP} result excludes the null mixing hypothesis at 3.3σ significance. This analysis is based on an integrated luminosity of 468 fb^{-1} collected with the BABAR detector at the PEP-II asymmetric-energy e^+e^- collider.

DOI: [10.1103/PhysRevD.87.012004](https://doi.org/10.1103/PhysRevD.87.012004)

PACS numbers: 13.25.Ft, 11.30.Er, 12.15.Ff

I. INTRODUCTION

Several measurements [1–6] show evidence for mixing in the D^0 - \bar{D}^0 system consistent with predictions of possible Standard Model (SM) contributions [7–11]. These results also constrain many new physics models [12–16]. An observation of CP violation (CPV) in the D^0 - \bar{D}^0 system at the present experimental sensitivity would provide possible evidence for physics beyond the SM [17–21].

*Now at the University of Tabuk, Tabuk 71491, Saudi Arabia.

†Also with Università di Perugia, Dipartimento di Fisica, Perugia, Italy.

‡Now at the University of Huddersfield, Huddersfield HD1 3DH, United Kingdom.

§Deceased.

||Now at University of South Alabama, Mobile, Alabama 36688, USA.

¶Also with Università di Sassari, Sassari, Italy.

One manifestation of $D^0\text{--}\bar{D}^0$ mixing is differing D^0 decay time distributions for decays to different CP eigenstates Ref. [22]. We present a measurement of charm mixing using the ratio of lifetimes obtained from the decays of neutral D mesons to CP -even and CP -mixed two-body final states. We also present a search for indirect CP violation arising from a difference in D^0 and \bar{D}^0 partial decay widths to CP -even eigenstates. Recently the LHCb Collaboration has reported evidence for CPV in the difference of the time-integrated CP asymmetries in $D^0 \rightarrow K^- K^+$ and $D^0 \rightarrow \pi^- \pi^+$ decays [23]. This measurement is primarily sensitive to direct CPV . As explained in Appendix A, we are not sensitive to effects of direct CP violation at the level of the result reported by LHCb, and we therefore assume no direct CPV in our baseline model.

We measure the effective D^0 lifetimes in three different two-body final states: $K^\pm \pi^\pm$, $K^- K^+$, and $\pi^- \pi^+$. We make no distinction between the Cabibbo-favored $D^0 \rightarrow K^- \pi^+$ and doubly Cabibbo-suppressed $D^0 \rightarrow K^+ \pi^-$ modes; in other words, we analyze and describe them together. Given the current experimental evidence indicating a small mixing rate, the lifetime distribution for all two-body final states is exponential to a good approximation. Decays in the $K^\pm \pi^\pm$ mode are to a CP -mixed final state, and are assumed to be described by the average D^0 width Γ . The singly Cabibbo-suppressed decays D^0 (\bar{D}^0) to the CP -even $K^- K^+$ and $\pi^- \pi^+$ final states are described by the partial decay rate Γ^+ ($\bar{\Gamma}^+$), where $+$ indicates the CP of the final state. We present in Appendix A a discussion of the mixing formalism leading to the expressions that are used to extract the mixing parameter y_{CP} and the CPV parameter ΔY ,

$$y_{CP} = \frac{\Gamma^+ + \bar{\Gamma}^+}{2\Gamma} - 1, \quad (1)$$

$$\Delta Y = \frac{\Gamma^+ - \bar{\Gamma}^+}{2\Gamma}, \quad (2)$$

from the experimentally measured CP -mixed and CP -even lifetimes. This definition of ΔY is opposite in sign to that in our previous measurement [2] and is now consistent with that used by the Heavy Flavor Averaging Group [24].

Tagged decays refer to D^0 mesons coming from $D^{*+} \rightarrow D^0 \pi^+$ decays [25], while untagged decays refer to D^0 mesons where no D^{*+} parent was found. The charge of the $D^{*\pm}$ is used to split the $K^- K^+$ and $\pi^- \pi^+$ samples into those originating from D^0 and from \bar{D}^0 mesons in order to measure the CP -violating parameter ΔY . The requirement of a D^{*+} parent strongly suppresses backgrounds; hence untagged decays are reconstructed only in $K^\pm \pi^\pm$ and $K^- K^+$ because of the relatively poor signal-to-background ratio in the untagged $\pi^- \pi^+$ final state. In summary, we study seven modes: two untagged and five tagged.

In addition to the increased integrated luminosity of the new dataset compared to that used in our earlier results [2,3], this analysis benefits from improved charged-particle track reconstruction, and a more inclusive and optimized event selection. The particle identification selection efficiency was sizably increased both for pions and kaons in the high-momentum-spectrum range by improving the algorithms that combine the information coming from the detector. We implement an improved background model, and we simultaneously fit both the tagged and untagged datasets.

II. EVENT RECONSTRUCTION AND SELECTION

We use 468 fb $^{-1}$ of $e^+ e^-$ colliding-beam data recorded at, and slightly below, the $Y(4S)$ resonance ($e^+ e^-$ center-of-mass [CM] energy $\sqrt{s} \sim 10.6$ GeV) with the BABAR detector [26] at the SLAC National Accelerator Laboratory PEP-II asymmetric-energy B Factory. To avoid potential bias, we finalize our data selection criteria, as well as the procedures for fitting, extracting statistical limits, and determining systematic uncertainties, prior to examining the results.

We reconstruct charged tracks and vertices with a five-layer, double-sided silicon vertex tracker (SVT) and a 40-layer drift chamber. We select D^0 candidates by pairing oppositely charged tracks, requiring each track to satisfy particle identification criteria based on specific ionization energy loss (dE/dx) from the SVT and drift chamber, and Cherenkov angle measurements from a ring-imaging Cherenkov detector. We then refit the D^0 daughter tracks, requiring them to originate from a common vertex. To reduce contributions from D^0 's produced via B -meson decay to a negligible level, we require each D^0 to have momentum in the CM frame $p_{CM} > 2.5$ GeV/ c .

For tagged decays, we reconstruct D^{*+} candidates by combining a D^0 candidate with a slow pion track π_s^+ , requiring them to originate from a common vertex constrained to the $e^+ e^-$ interaction region. We require the π_s^+ momentum to be greater than 0.1 GeV/ c in the laboratory frame and less than 0.45 GeV/ c in the CM frame. We reject a positron that fakes a π_s^+ candidate by using dE/dx information and veto any π_s^+ candidate that may have originated from a reconstructed photon conversion or π^0 Dalitz decay. The distribution of the difference Δm between the reconstructed D^{*+} and D^0 masses peaks near $\Delta m \sim 0.1455$ GeV/ c^2 . Backgrounds are suppressed by retaining only tagged candidates in the range $0.1447 < \Delta m < 0.1463$ GeV/ c^2 .

To determine the proper time t and its error σ_t for each D^0 candidate, we perform a combined fit to the D^0 production and decay vertices. We constrain the production point to be within the $e^+ e^-$ interaction region, which we determine using Bhabha and di-muon events from triggers close in time to any given signal candidate event. We retain only candidates with a χ^2 -based probability for the fit

$P(\chi^2) > 0.1\%$, and with $-2 < t < 4$ ps and $\sigma_t < 0.5$ ps. For tagged decays, this fit does not incorporate any π_s^+ information in order to ensure that the lifetime resolution models for tagged and untagged signal decays are very similar. The most probable value of σ_t for signal events is $\sim 40\%$ of the nominal D^0 lifetime [27].

If an event contains a tagged D^0 decay, we exclude all untagged D^0 candidates from that event in the final sample. For a given final state, when multiple D^0 (for the untagged modes) or D^{*+} (for the tagged modes) candidates in an event share one or more tracks, we retain only the candidate with the highest $P(\chi^2)$. The fraction of events with multiple D^0 candidates with overlapping daughter tracks is $\ll 1\%$ for all final states.

III. INVARIANT-MASS FITS

We characterize the D^0 invariant-mass (M) distribution for each of the seven modes with an extended unbinned maximum likelihood fit to D^0 and \bar{D}^0 samples. We allow the parameters governing the shapes of the probability density functions (PDFs), as well as the expected signal and background candidate yields, to vary in the fits. For the tagged CP -even modes we fit the D^0 and \bar{D}^0 samples simultaneously, sharing all parameters except for the expected signal and background candidate yields.

We fit the tagged $\pi^-\pi^+$ invariant-mass distribution in the fit range $1.82 < M_{\pi\pi} < 1.93$ GeV/c^2 using a sum of two Gaussians with independent means and widths for the signal PDF, along with a first-order Chebychev polynomial for the total background.

The fit model for the tagged K^-K^+ invariant-mass distribution is similar to $\pi^-\pi^+$, except that the fit range is $1.82 < M_{KK} < 1.91$ GeV/c^2 , and the signal PDF is the sum of two independent Gaussians and a modified Gaussian with a power-law tail [28], which aids in better modeling of the lower tail of the distribution.

The signal PDF for the untagged K^-K^+ mode and for both tagged and untagged $K^\pm\pi^\pm$ modes is a sum of three independent Gaussians: the background is modeled using a second-order Chebychev polynomial. The mass fit range is $1.82 < M_{KK} < 1.91$ GeV/c^2 for the untagged K^-K^+ mode, $1.81 < M_{K\pi} < 1.92$ GeV/c^2 for the untagged $K^\pm\pi^\pm$ mode, and $1.80 < M_{K\pi} < 1.93$ GeV/c^2 for the tagged $K^\pm\pi^\pm$ mode. In these modes, we do not distinguish D^0 from \bar{D}^0 candidates, and therefore determine only the total signal and total background yields, in addition to the signal and background shape parameters.

The reconstructed D^0 invariant-mass distributions and the fit results are shown in Fig. 1, together with a plot of the corresponding normalized Poisson pulls [29].

IV. SIGNAL AND SIDEBAND REGIONS

For the lifetime fit, we determine the regions in two-body invariant mass that maximize signal significance,

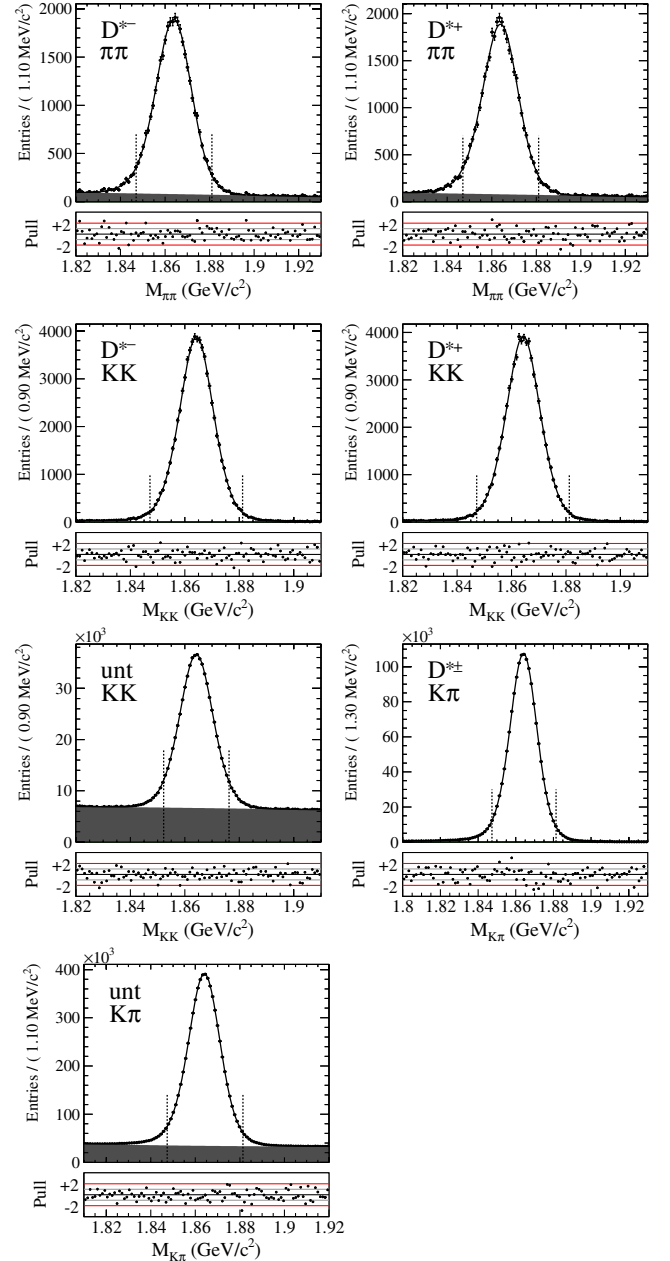


FIG. 1 (color online). The reconstructed two-body invariant-mass distributions for the seven modes. The vertical lines show the lifetime-fit mass region, defined in Sec. IV. The shaded regions are the background contributions. The normalized Poisson pulls for each fit are shown under each plot: “unt” refers to the untagged datasets.

minimize systematic effects due to backgrounds, and minimize the effect of the correlation between the D^0 invariant mass and proper time. We refer to these regions as the lifetime-fit mass regions. Based on these studies, the optimal lifetime-fit mass region is 34 MeV/c^2 wide for all tagged modes and untagged $K^\pm\pi^\pm$ events, $1.847 < M < 1.881$ GeV/c^2 . Because of the smaller signal-to-background ratio for the untagged K^-K^+ events, the lifetime-fit mass region for this mode is only 24 MeV/c^2 in width,

TABLE I. Expected composition (in %) of the misreconstructed-charm backgrounds. Only misreconstructed-charm background channels that have $>1\%$ contribution in at least one signal mode are listed. For the tagged modes, the yields are the sum of the separate D^0 and \bar{D}^0 tags.

Mode	Tagged Modes			Untagged Modes	
	$\pi^- \pi^+$	$K^- K^+$	$K^\mp \pi^\pm$	$K^- K^+$	$K^\mp \pi^\pm$
$D^0 \rightarrow X \ell \nu$	15.4	10.3	29.9	7.2	≤ 2
$D^0 \rightarrow K^- \pi^+$	80.8	14.9	57.1	8.8	35.8
$D^0 \rightarrow \pi^0 \pi^+ K^-$	1.1	70.3	1.7	63.3	6.9
$D^+ \rightarrow \pi^+ \pi^+ K^-$	≤ 1	2.9	≤ 1	11.8	≤ 2
$D^0 \rightarrow K^+ K^-$	≤ 1	≤ 1	1.3	≤ 1	3.5
$D^0 \rightarrow \pi^+ \pi^-$	1.8	≤ 1	2.2	≤ 1	3.1
$D^0 \rightarrow \pi^+ \pi^- \pi^0$	≤ 1	≤ 1	7.0	≤ 1	17.3
Λ decays	≤ 1	≤ 1	≤ 1	4.9	2.6

$1.852 < M < 1.876$ GeV/ c^2 . For the tagged modes, a mass difference sideband $0.151 < \Delta m < 0.159$ GeV/ c^2 is used, along with a low- (high-) invariant-mass sideband, 1.819 (1.890) $< M < 1.839$ (1.910) GeV/ c^2 . The low- (high-) mass sideband used for the untagged modes, 1.810 (1.899) $< M < 1.830$ (1.919) GeV/ c^2 , is displaced from the tagged sideband in order to reduce the signal component there. The contribution of the signal events in the sideband regions is in general very small compared to the background; however, it has been considered when extracting the combinatorial-background PDF. The signal purities in the lifetime-fit mass regions range from $\sim 75\%$ for the untagged $K^- K^+$ sample to $\sim 99.8\%$ for the tagged $K^\mp \pi^\pm$ events.

We classify D^0 candidate decays in the lifetime-fit mass region as follows: D^0 signal decays; misreconstructed-charm decays, i.e., those in which the candidate- D^0 daughter tracks are decay products of a nonsignal weak charm decay; and random combinatorial background. Table I gives the composition of the misreconstructed-charm backgrounds expected from simulated events [30] in each final state.

V. LIFETIME FIT

The lifetimes are determined from an extended unbinned maximum likelihood fit to t and σ_t for candidates in the lifetime-fit mass region. All modes are fit simultaneously using shared signal-resolution-function parameters. The signal, misreconstructed-charm, and combinatorial components are described by their own set of PDFs, which in the tagged modes can also depend on the charm flavor.

The lifetime PDF for the signal is an exponential function convolved with a resolution function, which is the sum of three Gaussian functions whose widths are proportional to σ_t . The explicit form of the signal lifetime PDF is

$$\begin{aligned} \mathcal{R}_{F,L}^T(t, \sigma_t) = & f_{i1} \mathcal{D}(t, \sigma_t; S'_T S_F s_1, t_0, \tau_L) \\ & + (1 - f_{i1}) [f_{i2} \mathcal{D}(t, \sigma_t; S'_T S_F s_2, t_0, \tau_L) \\ & + (1 - f_{i2}) \mathcal{D}(t, \sigma_t; S'_T S_F s_3, t_0, \tau_L)], \end{aligned} \quad (3)$$

where f_{ii} (with $i = 1, 2$) parametrizes the contribution of each individual Gaussian, s_i (with $i = 1, 2, 3$) is a scaling factor associated with each Gaussian, and t_0 is an offset of the mean of the resolution function. The function $\mathcal{D}(t, \sigma_t; s, t_0, \tau)$ is given by

$$\begin{aligned} \mathcal{D}(t, \sigma_t; s, t_0, \tau) = & C_{\sigma_t} \int \exp(-t_{\text{true}}/\tau) \\ & \times \exp\left(-\frac{(t - t_{\text{true}} + t_0)^2}{2(s \cdot \sigma_t)^2}\right) dt_{\text{true}}, \end{aligned} \quad (4)$$

where the normalization coefficient C_{σ_t} is chosen such that

$$\int \mathcal{D}(t, \sigma_t; s, t_0, \tau) dt = 1 \quad \text{for each } \sigma_t. \quad (5)$$

With this definition, the product $H_{\sigma_t}^{\text{sig}}(\sigma_t) \cdot \mathcal{D}(t, \sigma_t; s, t_0, \tau)$ is a properly normalized two-dimensional conditional PDF, where $H_{\sigma_t}^{\text{sig}}(\sigma_t)$ is a PDF characterizing the σ_t distribution, described below. To account for small differences in the resolution function for the different final states we introduce additional mode-dependent scale factors S_F , $F = K\pi, KK, \pi\pi$. We also allow for differences between the resolution functions for tagged and untagged modes by means of scale factors S'_T , $T = \text{tag (tagged) or unt (untagged)}$. We fix $S_{K\pi}$ and S'_{unt} to 1.

The three lifetime parameters are $\tau_L = \{\tau^+, \bar{\tau}^+, \tau_{K\pi}\}$, where $\tau_{K\pi}$ is extracted from the tagged and untagged $K^\mp \pi^\pm$ modes, while τ^+ and $\bar{\tau}^+$ are extracted from the tagged and untagged CP -even modes. Approximately 0.4% of the tagged CP -even samples contain correctly reconstructed D^0 candidates combined with an unrelated π_s^+ : this fraction has been estimated from simulated events and verified in data by an earlier BABAR analysis [1]. These candidates have the same resolution and lifetime behavior as those from correctly reconstructed D^{*+} decays, but about half of them will be tagged as the wrong flavor. Therefore, the tagged CP -even D^0 proper-time distributions are modeled as the weighted sum of PDFs for correctly tagged and untagged candidates, characterized by the lifetime parameters τ^+ and $\bar{\tau}^+$, respectively, and a mistag fraction $f_{\text{tag}} = 0.2\%$. The tagged CP -even \bar{D}^0 proper-time distributions are modeled in a similar fashion, where now the correctly tagged and mistagged PDFs are characterized by the lifetime parameters $\bar{\tau}^+$ and τ^+ , respectively. The untagged $K^- K^+$ proper-time distribution is modeled as a weighted sum of two PDFs characterized by the lifetime parameters τ^+ and $\bar{\tau}^+$, respectively, and a weighting fraction $f_{D^0} = 0.5$. These parametrizations assume no direct CPV , and allow for CPV in the interference between decays with and without mixing characterized by a mode-independent weak phase ϕ . Both f_{tag} and

f_{D^0} are varied as part of the systematic error estimate for y_{CP} and ΔY . All five tagged and two untagged signal-lifetime PDFs are explicitly given in Appendix B.

The σ_t PDF for signal candidates is obtained directly from data by subtracting the sum of the background σ_t distributions from that of all candidates in the lifetime-fit mass region. These one-dimensional σ_t distributions are used to model the $H_{\sigma_t}^{\text{sig}}(\sigma_t)$ PDF discussed previously.

We determine the t versus σ_t misreconstructed-charm signal-like PDF shape parameters and yields by fitting simulated events in the lifetime-fit mass region and then fix these parameters in the lifetime fit to data. We vary the lifetimes and yields as part of the study of systematic effects.

The largest background in the lifetime-fit mass region is due to random combinations of tracks. The PDF describing the two-dimensional combinatorial background in t and σ_t in the lifetime-fit mass region is characterized as a weighted average of the two-dimensional PDFs extracted from the mass sideband regions. The weights for the low and high sidebands are obtained from simulated events. The (t, σ_t) combinatorial PDF in each sideband and for each mode, except for the untagged K^-K^+ mode, is extracted as a two-dimensional histogram from the sideband samples. From these histograms we subtract the contribution of signal and misreconstructed-charm backgrounds, each of which is estimated from simulated events, to obtain the final combinatorial PDF in each sideband. For the untagged K^-K^+ mode, a similar procedure is used but, instead of histograms, analytic signal-like PDFs are used. For the background PDFs the offsets and the lifetimes are allowed to be different for each Gaussian. The signal and misreconstructed-charm PDF parameters are extracted by fitting simulated events, and then fixed, along with the expected candidate yields, in the fit that extracts the combinatorial PDFs in each sideband.

For the untagged K^-K^+ mode both the expected signal and combinatorial yields are free parameters in the lifetime fit. The expected combinatorial background yields in the other modes are determined by integrating the total background PDF extracted from the mass fit in the lifetime-fit mass region, and then subtracting the expected misreconstructed-charm background yields, which are

TABLE II. Signal and background yields in the lifetime-fit mass region. Yields with uncertainties are those obtained directly from the lifetime fit to data. For the tagged modes, the yields are the sum of the separate D^0 and \bar{D}^0 tags.

	Tagged Modes			Untagged Modes	
	$\pi^- \pi^+$	$K^- K^+$	$K^\mp \pi^\pm$	$K^- K^+$	$K^\mp \pi^\pm$
Signal	65 430 ± 260	136 870 ± 370	1 487 000 ± 1200	496 200 ± 1200	5 825 300 ± 2600
Comb. Bkgd.	3760	653	2849	165 000 ± 1000	1 044 552
Charm Bkgd.	97	309	642	5477	4645

determined from samples of simulated events. A small bias on these fit yields is observed in fits to simulated events. To correct for this, we scale the data yields based on the simulated-event fits and vary the mode-dependent scale factors as a systematic uncertainty. Table II gives

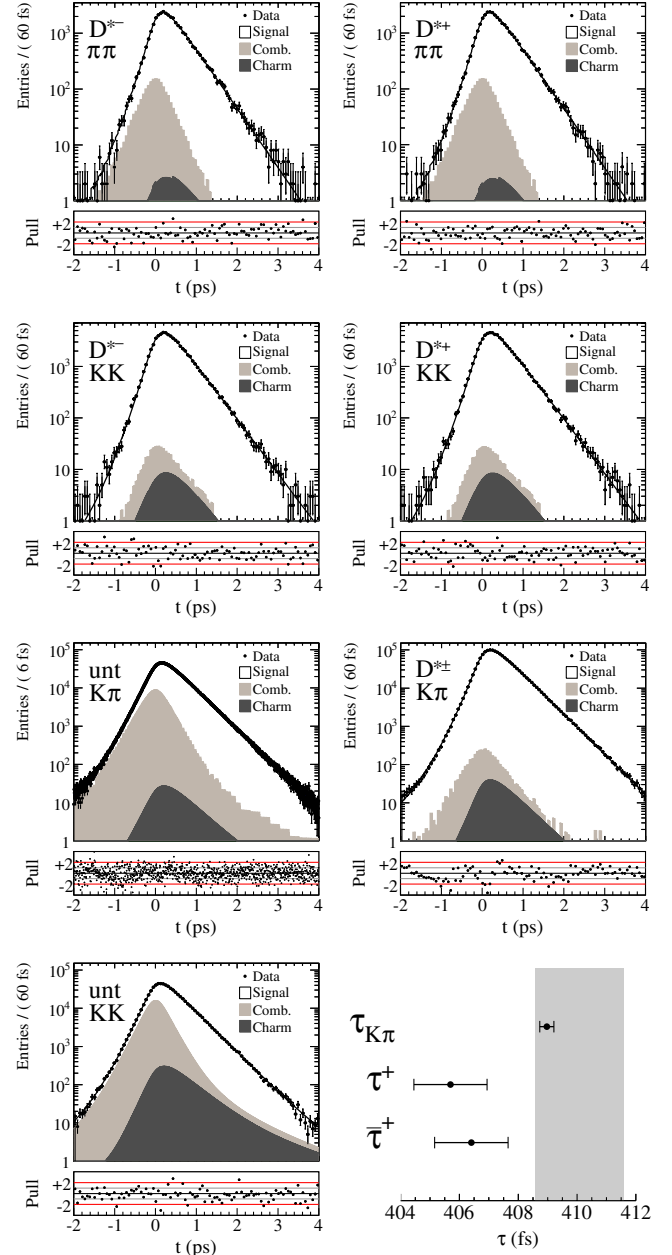


FIG. 2 (color online). Proper-time t distribution for each decay mode with the fit results overlaid. The combinatorial distribution (indicated as “Comb.” in light gray) is stacked on top of the misreconstructed-charm distribution (indicated as “Charm” in dark gray). The normalized Poisson pulls for each fit are shown under each plot: “unt” refers to the untagged datasets. The bottom right plot shows the individual lifetimes (with statistical uncertainties only): the gray band indicates the PDG D^0 lifetime $\pm 1\sigma$ [27].

the event-class yields plus uncertainties obtained from the lifetime fit and indicates the yields that are fixed.

The simultaneous fit to all events in the lifetime-fit mass region has 20 floating parameters: the seven signal yields and three signal lifetimes; the yield of untagged K^-K^+ combinatorial candidates; the offset t_0 ; the parameters f_{t1} and f_{t2} characterizing the weight of each Gaussian in the signal resolution mode; and the proper-time error scaling parameters $s_1, s_2, s_3, S_{KK}, S_{\pi\pi}$, and S'_{tag} . After extracting the three signal lifetimes, using their reciprocals in the computation of y_{CP} and ΔY as defined in Eqs. (1) and (2), respectively, we find

$$y_{CP} = [0.72 \pm 0.18(\text{stat})]\%,$$

$$\Delta Y = [0.09 \pm 0.26(\text{stat})]\%.$$

The statistical errors are computed using the covariance matrix returned by the fit. The lifetime-fit mass region proper-time distributions and projections of the lifetime fit for the seven different decay modes are shown in Fig. 2.

VI. CROSS CHECKS AND SYSTEMATICS

We have performed numerous cross checks to search for potential problems, in addition to quantitative studies that yield the systematic uncertainties given in Table III, discussed below. Initially, we tested the fit model by generating large ensembles of data sets randomly drawn from the underlying total PDF, and observed no biases in the y_{CP} and ΔY results obtained. In addition, we have fit an ensemble of four simulated data sets, each equivalent in luminosity to the data, and found no evidence of bias in y_{CP} or ΔY .

In fitting the data, we find that the tagged and untagged extracted lifetimes for K^-K^+ , and separately for $K^\pm\pi^\pm$, are compatible within the statistical uncertainties. We performed a simultaneous fit to the tagged channels, and a

separate simultaneous fit to the untagged channels, and find the lifetimes to be compatible within the statistical uncertainties. We repeated the fit allowing the K^-K^+ and $\pi^-\pi^+$ final states to have separate τ^+ and $\bar{\tau}^+$ lifetimes, and observed no statistically significant difference between the K^-K^+ and $\pi^-\pi^+$ results. We estimated the effects of the SVT misalignment to be negligible.

We varied the lifetime-fit mass region width by ± 4 and ± 2 MeV/ c^2 . We adopt as the systematic uncertainty half the rms of the differences $|\Delta[y_{CP}]|$ and $|\Delta[\Delta Y]|$ from the nominal-fit central values. We also shifted the position of each mass region by centering each of them at the most probable value for the signal PDF obtained in the invariant-mass fits. These systematic uncertainties are given in the first two lines of Table III.

For the untagged K^-K^+ mode, the combinatorial yield is a parameter determined in the lifetime fit. However, it is also needed to determine the signal σ_i PDF. We first use the total background yield determined from the mass fit to extract a signal σ_i PDF, which is employed in an initial simultaneous lifetime fit. The combinatorial yield from this fit is used to construct an improved σ_i signal PDF and a second fit is performed (the nominal fit). We estimate the systematic error on y_{CP} and ΔY associated with the determination of the signal σ_i PDF for the untagged K^-K^+ mode to be the difference in the values obtained from an additional iteration of the fit and the nominal fit.

We vary the nominal mistag rate of 0.2% by $\pm 0.04\%$, a 20% relative variation, and find no significant change in the nominal fit values. Instead of assuming equal fractions of D^0 and \bar{D}^0 in the untagged K^-K^+ mode, we adopt the latest CDF result for direct CPV [32], and find negligible change in y_{CP} and ΔY .

We rely on simulated events to determine both the PDF shapes and yields for the misreconstructed-charm backgrounds. To account for the model dependence, we vary the effective lifetime of these events by $\pm 5\%$, except for the tagged $\pi^-\pi^+$ mode where the variation is $\pm 15\%$ due to the small number of simulated events that pass the selection criteria for this mode. We also vary the expected misreconstructed-charm yields by $\pm 10\%$ in the tagged channels, and $\pm 5\%$ in the untagged channels. Each variation is simultaneously applied to all modes. These are $\geq 2\sigma$ variations relative to the statistical uncertainties of the simulated data sets.

We vary the yields, weighting parameters, and fitting strategy used to obtain the two-dimensional lifetime PDF for combinatorial-background events in the lifetime-fit mass region from the mass sidebands. The yields for the tagged combinatorial-background events are varied by $\sim 5\%$ in the $\pi^-\pi^+$ mode, 15% in tagged K^-K^+ , and 20% in $K^\pm\pi^\pm$. The untagged $K^\pm\pi^\pm$ combinatorial-background yield is varied using the value extracted from an alternative lifetime-fit model in which the yield is allowed to vary.

TABLE III. The y_{CP} and ΔY systematic uncertainties. The total is the sum-in-quadrature of the entries in each column.

Fit Variation	$ \Delta[y_{CP}] $ (%)	$ \Delta[\Delta Y] $ (%)
mass window width	0.057	0.022
mass window position	0.005	0.001
untagged KK signal σ_i PDF	0.022	0.000
mistag fraction	0.000	0.000
untagged $KK D^0$ fraction	0.001	0.000
charm bkgd. lifetimes	0.042	0.001
charm bkgd. yields	0.016	0.000
comb. yields	0.043	0.002
comb. sideband weights	0.004	0.001
comb. PDF shape	0.066	0.000
σ_i selection	0.052	0.053
candidate selection	0.028	0.011
Total	0.124	0.058

The weights given to the low- and high-mass sidebands in the data in order to derive the combinatorial PDF in the lifetime-fit mass region in the data are extracted from simulated events. They are varied by plus and minus the statistical uncertainty derived from splitting the simulated data set, which is equivalent to several times the nominal integrated luminosity, into data sets that numerically match the nominal luminosity.

We also apply the variations described above for the misreconstructed-charm background to vary the yields and shape of the PDF that describe the residual signal events in the sidebands. This is also done for the misreconstructed-charm PDF used in the sideband fits from which the two-dimensional combinatorial PDF is extracted. This yields the combinatorial PDF shape variation, which is then used in the nominal fit to obtain the variation reported in Table III.

Finally, we vary the σ_t criteria by ± 0.1 ps from the nominal $\sigma_t < 0.5$ ps, and take as the systematic uncertainty the rms of the deviations from the nominal-fit central value divided by $\sqrt{2}$. We also consider two variations in how multiple candidates sharing one or more daughter tracks are treated. In the first variation, we retain all multiple candidates if each candidate passes all the other selection criteria. In the second variation, we reject all multiple candidates sharing one or more daughter tracks. We fit these data sets using the nominal-fit model, and assign the largest observed deviation from the nominal y_{CP} and ΔY central values as the systematic uncertainty in Table III. The total y_{CP} and ΔY systematic uncertainties are calculated by summing the contributions from all sources in quadrature, and are reported in the last row of Table III.

VII. CONCLUSIONS

In summary, we measured y_{CP} and ΔY to a precision significantly better than our previous measurements [2,3]. Both results are more precise than, and consistent with, the weighted average of all previous measurements [24], when the previous *BABAR* results are excluded. We obtain

$$y_{CP} = [0.72 \pm 0.18(\text{stat}) \pm 0.12(\text{syst})]\%,$$

$$\Delta Y = [0.09 \pm 0.26(\text{stat}) \pm 0.06(\text{syst})]\%.$$

We exclude the null mixing hypothesis at 3.3σ significance, and find no evidence for CPV . Our results are consistent with the world average value of the mixing parameter y obtained from $D^0 \rightarrow K_S^0 h^- h^+$ (where $h = K, \pi$) [24], as expected in the absence of CPV . The y_{CP} measurement is the most precise single measurement to date, with significant improvements on the statistical and systematic error with respect to the previous most precise measurement [3] $y_{CP} = (1.16 \pm 0.22 \pm 0.18)\%$.

The value of ΔY obtained here is consistent with our previously published result [2] when the same definition is used in both cases. The new y_{CP} value is consistent with

our previous result [3] with a probability of $\geq 2\%$, assuming that the systematics for both the old and new measurements are fully correlated, and taking into account the fact that $\sim 40\%$ of the events in the current sample are also present in the samples used in the previous measurements [2,3]. The results here supersede the previous *BABAR* results for these modes [2,3].

ACKNOWLEDGMENTS

We are grateful for the extraordinary contributions of our PEP-II colleagues in achieving the excellent luminosity and machine conditions that have made this work possible. The success of this project also relies critically on the expertise and dedication of the computing organizations that support *BABAR*. The collaborating institutions wish to thank SLAC for its support and the kind hospitality extended to them. This work is supported by the US Department of Energy and National Science Foundation, the Natural Sciences and Engineering Research Council (Canada), the Commissariat à l’Energie Atomique and Institut National de Physique Nucléaire et de Physique des Particules (France), the Bundesministerium für Bildung und Forschung and Deutsche Forschungsgemeinschaft (Germany), the Istituto Nazionale di Fisica Nucleare (Italy), the Foundation for Fundamental Research on Matter (The Netherlands), the Research Council of Norway, the Ministry of Education and Science of the Russian Federation, Ministerio de Ciencia e Innovación (Spain), and the Science and Technology Facilities Council (United Kingdom). Individuals have received support from the Marie-Curie IEF program (European Union) and the A. P. Sloan Foundation (USA).

APPENDIX A: MIXING FORMALISM AND CONSIDERATIONS ON THE ROLE OF DIRECT CP VIOLATION

In the following we briefly review the mixing formalism [27] considering the possible effects of direct CPV on the y_{CP} and ΔY observables.

The time evolution of the flavor eigenstates D^0 and \bar{D}^0 is governed by the Schrödinger equation:

$$i \frac{\partial}{\partial t} \begin{pmatrix} D^0(t) \\ \bar{D}^0(t) \end{pmatrix} = \left(\mathbf{M} - \frac{i}{2} \mathbf{\Gamma} \right) \begin{pmatrix} D^0(t) \\ \bar{D}^0(t) \end{pmatrix}. \quad (\text{A1})$$

The mass eigenstates D_1 and D_2 are obtained from the diagonalization of the effective Hamiltonian $\mathcal{H}_{\text{eff}} = \mathbf{M} - \frac{i}{2} \mathbf{\Gamma}$. Under the hypothesis of CPT conservation the two mass eigenstates can be written in terms of the flavor eigenstates as

$$|D_1\rangle = p|D^0\rangle + q|\bar{D}^0\rangle, \quad |D_2\rangle = p|D^0\rangle - q|\bar{D}^0\rangle, \quad (\text{A2})$$

where

$$\left(\frac{q}{p}\right)^2 = \frac{M_{12}^* - \frac{i}{2}\Gamma_{12}^*}{M_{12} - \frac{i}{2}\Gamma_{12}} \quad \text{and} \quad |p|^2 + |q|^2 = 1. \quad (\text{A3})$$

We choose the positive root for q/p : choosing the negative one just means exchanging D_1 with D_2 . If $CP|D^0\rangle = +|\bar{D}^0\rangle$, in the case of no CPV , D_1 is the CP -even state and D_2 the CP -odd state.

It is traditional to quantify the size of D^0 - \bar{D}^0 mixing in terms of the parameters $x \equiv \Delta m/\Gamma$ and $y \equiv \Delta\Gamma/2\Gamma$, where $\Delta m = m_1 - m_2$ ($\Delta\Gamma = \Gamma_1 - \Gamma_2$) is the difference in mass (width) of the states defined in Eq. (A2) and $\Gamma = (\Gamma_1 + \Gamma_2)/2$ is the average width. If either x or y is nonzero, mixing will occur. While most SM expectations for the size of both are $\lesssim 10^{-3}$ [10,33], values as high as 10^{-2} or even higher are predicted by certain models [13,15].

CP violation can manifest in D^0 decays in three ways:

- (i) in decay, when $|A_f/\bar{A}_f| \neq 1$,
- (ii) in mixing, when $r_m = |q/p| \neq 1$,
- (iii) in the interference between decays with and without mixing, when the weak phase ϕ_f of $\lambda_f \equiv \frac{q}{p} \frac{\bar{A}_f}{A_f}$ is different from zero,

where A_f (\bar{A}_f) is the amplitude for D^0 (\bar{D}^0) decaying into a final state f , $A_f \equiv \langle f | \mathcal{H}_D | D^0 \rangle$ ($\bar{A}_f \equiv \langle f | \mathcal{H}_D | \bar{D}^0 \rangle$).

The presence of mixing alters the exponential distribution for the D^0 decay into a final state f . In particular we have

$$\begin{aligned} \Gamma(D^0(t) \rightarrow f) = & \frac{1}{2} |A_f|^2 e^{-\Gamma t} [(1 + |\lambda_f|^2) \cosh \Gamma t \\ & + (1 - |\lambda_f|^2) \cos x \Gamma t - 2\Re(\lambda_f) \sinh \Gamma t \\ & + 2\Im(\lambda_f) \sin x \Gamma t], \end{aligned} \quad (\text{A4})$$

$$\begin{aligned} \Gamma(\bar{D}^0(t) \rightarrow f) = & \frac{1}{2} |\bar{A}_f|^2 e^{-\Gamma t} [(1 + |\lambda_f^{-1}|^2) \cosh \Gamma t \\ & + (1 - |\lambda_f^{-1}|^2) \cos x \Gamma t - 2\Re(\lambda_f^{-1}) \sinh \Gamma t \\ & + 2\Im(\lambda_f^{-1}) \sin x \Gamma t]. \end{aligned} \quad (\text{A5})$$

In this analysis we are interested in CP -even final states ($f = h^+ h^-$, $h = K, \pi$). If we neglect second-order terms in $x\Gamma t$ and $y\Gamma t$, the decay time distributions can be treated as exponentials with effective widths [34]:

$$\begin{aligned} \Gamma(D^0(t) \rightarrow f) & \propto e^{-\Gamma_{hh}^+ t} \quad \text{with} \\ \Gamma_{hh}^+ & = \Gamma[1 + y\Re(\lambda_{hh}) - x\Im(\lambda_{hh})], \end{aligned} \quad (\text{A6})$$

$$\begin{aligned} \Gamma(\bar{D}^0(t) \rightarrow f) & \propto e^{-\bar{\Gamma}_{hh}^+ t} \quad \text{with} \\ \bar{\Gamma}_{hh}^+ & = \Gamma[1 + y\Re(\lambda_{hh}^{-1}) - x\Im(\lambda_{hh}^{-1})]. \end{aligned} \quad (\text{A7})$$

To better understand the effects of CP violation we introduce two more parameters, one describing CPV in decay (A_D^f) and one in mixing (A_M):

$$A_D^f = \frac{|A_f/\bar{A}_f|^2 - |\bar{A}_f/A_f|^2}{|A_f/\bar{A}_f|^2 + |\bar{A}_f/A_f|^2}, \quad (\text{A8})$$

$$A_M = \frac{r_m^2 - r_m^{-2}}{r_m^2 + r_m^{-2}}. \quad (\text{A9})$$

Since $f = h^+ h^-$, then $f = \bar{f}$. Noting that there is no strong phase in λ_f since the final state is its own CP conjugate, we can express λ_{hh} in terms of A_D^{hh} , A_M , and the CP -violating phase ϕ_{hh} :

$$\lambda_{hh} = \left[\frac{1 - A_D^{hh}}{1 + A_D^{hh}} \frac{1 + A_M}{1 - A_M} \right]^{1/4} e^{i\phi_{hh}}. \quad (\text{A10})$$

Expanding Eqs. (A6) and (A7), and retaining only terms up to first order in A_D^{hh} and A_M , we obtain

$$\begin{aligned} \Gamma_{hh}^+ & \simeq \Gamma \left[1 + (y \cos \phi_{hh} - x \sin \phi_{hh}) \right. \\ & \quad + \frac{1}{2} (A_M - A_D^{hh}) (y \cos \phi_{hh} - x \sin \phi_{hh}) \\ & \quad \left. - \frac{1}{4} A_M A_D^{hh} (y \cos \phi_{hh} - x \sin \phi_{hh}) \right], \end{aligned} \quad (\text{A11})$$

$$\begin{aligned} \bar{\Gamma}_{hh}^+ & \simeq \Gamma \left[1 + (y \cos \phi_{hh} + x \sin \phi_{hh}) \right. \\ & \quad - \frac{1}{2} (A_M - A_D^{hh}) (y \cos \phi_{hh} + x \sin \phi_{hh}) \\ & \quad \left. - \frac{1}{4} A_M A_D^{hh} (y \cos \phi_{hh} + x \sin \phi_{hh}) \right]. \end{aligned} \quad (\text{A12})$$

Combining the widths defined above we obtain the two observables y_{CP}^{hh} and ΔY^{hh} , which, in general, depend on the final state because of the CPV parameters A_D^{hh} and ϕ_{hh} :

$$y_{CP}^{hh} = \frac{\Gamma_{hh}^+ + \bar{\Gamma}_{hh}^+}{2\Gamma} - 1, \quad (\text{A13})$$

$$\Delta Y^{hh} = \frac{\Gamma_{hh}^+ - \bar{\Gamma}_{hh}^+}{2\Gamma}. \quad (\text{A14})$$

Other experiments characterize the CP -violating observable as A_Γ^{hh} ,

$$A_\Gamma^{hh} = \frac{\Gamma_{hh}^+ - \bar{\Gamma}_{hh}^+}{\Gamma_{hh}^+ + \bar{\Gamma}_{hh}^+}. \quad (\text{A15})$$

The relationship between A_Γ^{hh} , ΔY^{hh} , and y_{CP}^{hh} is

$$\Delta Y^{hh} = (1 + y_{CP}^{hh}) A_\Gamma^{hh}. \quad (\text{A16})$$

These quantities are directly related to the fundamental parameters that govern mixing and CPV in the charm sector:

$$y_{CP}^{hh} = y \cos \phi_{hh} - \frac{1}{2} [A_M - A_D^{hh}] x \sin \phi_{hh} - \frac{1}{4} A_M A_D^{hh} y \cos \phi_{hh}, \quad (\text{A17})$$

$$\Delta Y^{hh} = -x \sin \phi_{hh} + \frac{1}{2} [A_M - A_D^{hh}] y \cos \phi_{hh} + \frac{1}{4} A_M A_D^{hh} x \sin \phi_{hh}. \quad (\text{A18})$$

Both y_{CP}^{hh} and ΔY^{hh} are zero if there is no $D^0 - \bar{D}^0$ mixing. Otherwise, a nonzero value of y_{CP}^{hh} implies mixing and a nonzero value of ΔY^{hh} implies CPV .

In the charm sector, because the CKM elements involved belong to the Cabibbo submatrix, we can assume that the weak phase ϕ_{hh} does not depend on the final state: $\phi_{hh} = \phi$ [35]. As stated earlier, if direct CPV has a significant effect, then the values of y_{CP}^{hh} and ΔY^{hh} depend on the final state. In this analysis we assume that the effect of direct CPV is negligible in the decays to CP eigenstates; i.e., we assume $\Gamma_{KK}^+ = \Gamma_{\pi\pi}^+$ (and $\bar{\Gamma}_{KK}^+ = \bar{\Gamma}_{\pi\pi}^+$). In Eqs. (A11) and (A12) this means neglecting the linear terms in A_D^{hh} . Assuming that A_D^{hh} and y are both $\mathcal{O}(1\%)$ and $\phi_{hh} = 0$, the neglected term is $\mathcal{O}(10^{-4})$, beyond any current experimental sensitivity.

Under the above assumptions, Eqs. (A11) and (A12) become

$$\Gamma^+ \simeq \Gamma \left[1 + (y \cos \phi - x \sin \phi) + \frac{A_M}{2} (y \cos \phi - x \sin \phi) \right], \quad (\text{A19})$$

$$\bar{\Gamma}^+ \simeq \Gamma \left[1 + (y \cos \phi + x \sin \phi) - \frac{A_M}{2} (y \cos \phi + x \sin \phi) \right]. \quad (\text{A20})$$

Inserting Eqs. (A19) and (A20) into Eqs. (1) and (2) yields

$$y_{CP} = y \cos \phi - \frac{A_M}{2} x \sin \phi, \quad (\text{A21})$$

$$\Delta Y = -x \sin \phi + \frac{A_M}{2} y \cos \phi. \quad (\text{A22})$$

From the experimental point of view, we measure three lifetimes instead of the partial widths:

- (i) τ^+ for the $D^0 \rightarrow K^- K^+$, $\pi^- \pi^+$ decays,
- (ii) $\bar{\tau}^+$ for the $\bar{D}^0 \rightarrow K^- K^+$, $\pi^- \pi^+$ decays,
- (iii) $\tau_{K\pi}$ for the D^0 (and \bar{D}^0) $\rightarrow K^\mp \pi^\pm$ decays (the Cabibbo-favored $K^- \pi^+$ and the doubly Cabibbo-suppressed $K^+ \pi^-$ decays are collected in the same sample),

and use their inverse to compute y_{CP} and ΔY .

The measured observables constrain the parameters that govern mixing and indirect CPV in the charm sector.

APPENDIX B: SIGNAL-LIFETIME PDFS

The explicit form of the signal-lifetime PDFs based on the prototype PDFs presented in the main text are given below:

$$\mathcal{P}_{\pi\pi}^{D^{*+}}(t, \sigma_t) = (1 - f_{\text{tag}}^+) \mathcal{R}_{\pi\pi}^{\text{tag}}(t, \sigma_t; S_{\pi\pi} S'_{\text{tag}} s_i, t_0, \tau^+) + f_{\text{tag}}^+ \mathcal{R}_{\pi\pi}^{\text{tag}}(t, \sigma_t; S_{\pi\pi} S'_{\text{tag}} s_i, t_0, \bar{\tau}^+),$$

$$\mathcal{P}_{\pi\pi}^{D^{*-}}(t, \sigma_t) = (1 - f_{\text{tag}}^-) \mathcal{R}_{\pi\pi}^{\text{tag}}(t, \sigma_t; S_{\pi\pi} S'_{\text{tag}} s_i, t_0, \bar{\tau}^+) + f_{\text{tag}}^- \mathcal{R}_{\pi\pi}^{\text{tag}}(t, \sigma_t; S_{\pi\pi} S'_{\text{tag}} s_i, t_0, \tau^+),$$

$$\mathcal{P}_{KK}^{D^{*+}}(t, \sigma_t) = (1 - f_{\text{tag}}^+) \mathcal{R}_{KK}^{\text{tag}}(t, \sigma_t; S_{KK} S'_{\text{tag}} s_i, t_0, \tau^+) + f_{\text{tag}}^+ \mathcal{R}_{KK}^{\text{tag}}(t, \sigma_t; S_{KK} S'_{\text{tag}} s_i, t_0, \bar{\tau}^+),$$

$$\mathcal{P}_{KK}^{D^{*-}}(t, \sigma_t) = (1 - f_{\text{tag}}^-) \mathcal{R}_{KK}^{\text{tag}}(t, \sigma_t; S_{KK} S'_{\text{tag}} s_i, t_0, \bar{\tau}^+) + f_{\text{tag}}^- \mathcal{R}_{KK}^{\text{tag}}(t, \sigma_t; S_{KK} S'_{\text{tag}} s_i, t_0, \tau^+),$$

$$\mathcal{P}_{K\pi}^{D^{*\pm}}(t, \sigma_t) = \mathcal{R}_{K\pi}^{\text{tag}}(t, \sigma_t; S_{K\pi} S'_{\text{tag}} s_i, t_0, \tau_{K\pi}),$$

$$\mathcal{P}_{KK}^{\text{unt}}(t, \sigma_t) = (1 - f_{D^0}) \mathcal{R}_{KK}^{\text{unt}}(t, \sigma_t; S_{KK} S'_{\text{unt}} s_i, t_0, \bar{\tau}^+) + f_{D^0} \mathcal{R}_{KK}^{\text{unt}}(t, \sigma_t; S_{KK} S'_{\text{unt}} s_i, t_0, \tau^+),$$

$$\mathcal{P}_{K\pi}^{\text{unt}}(t, \sigma_t) = \mathcal{R}_{K\pi}^{\text{unt}}(t, \sigma_t; S_{K\pi} S'_{\text{unt}} s_i, t_0, \tau_{K\pi}),$$

where $f_{\text{tag}}^\pm = 0.2\%$, $f_{D^0} = 0.5$, and $S_{K\pi} = S'_{\text{unt}} = 1$ are fixed in the nominal fit.

- [1] B. Aubert *et al.* (BABAR Collaboration), *Phys. Rev. Lett.* **98**, 211802 (2007).
- [2] B. Aubert *et al.* (BABAR Collaboration), *Phys. Rev. D* **78**, 011105 (2008).

- [3] B. Aubert *et al.* (BABAR Collaboration), *Phys. Rev. D* **80**, 071103 (2009).
- [4] M. Staric *et al.* (Belle Collaboration), *Phys. Rev. Lett.* **98**, 211803 (2007).

- [5] L. M. Zhang *et al.* (Belle Collaboration), *Phys. Rev. Lett.* **99**, 131803 (2007).
- [6] T. Aaltonen *et al.* (CDF Collaboration), *Phys. Rev. Lett.* **100**, 121802 (2008).
- [7] L. Wolfenstein, *Phys. Lett.* **164B**, 170 (1985).
- [8] J. F. Donoghue, E. Golowich, B. R. Holstein, and J. Trampetic, *Phys. Rev. D* **33**, 179 (1986).
- [9] I. I. Bigi and N. G. Uraltsev, *Nucl. Phys.* **B592**, 92 (2000).
- [10] A. F. Falk, Y. Grossman, Z. Ligeti, and A. A. Petrov, *Phys. Rev. D* **65**, 054034 (2002).
- [11] A. F. Falk, Y. Grossman, Z. Ligeti, Y. Nir, and A. A. Petrov, *Phys. Rev. D* **69**, 114021 (2004).
- [12] G. Burdman and I. Shipsey, *Annu. Rev. Nucl. Part. Sci.* **53**, 431 (2003).
- [13] A. A. Petrov, *Int. J. Mod. Phys. A* **21**, 5686 (2006).
- [14] E. Golowich, S. Pakvasa, and A. A. Petrov, *Phys. Rev. Lett.* **98**, 181801 (2007).
- [15] E. Golowich, J. Hewett, S. Pakvasa, and A. A. Petrov, *Phys. Rev. D* **76**, 095009 (2007).
- [16] E. Golowich, J. Hewett, S. Pakvasa, and A. A. Petrov, *Phys. Rev. D* **79**, 114030 (2009).
- [17] G. Blaylock, A. Seiden, and Y. Nir, *Phys. Lett. B* **355**, 555 (1995).
- [18] G. Isidori, J. F. Kamenik, Z. Ligeti, and G. Perez, *Phys. Lett. B* **711**, 46 (2012).
- [19] Y. Hochberg and Y. Nir, *Phys. Rev. Lett.* **108**, 261601 (2012).
- [20] H.-Y. Cheng and C.-W. Chiang, *Phys. Rev. D* **85**, 034036 (2012).
- [21] G. F. Giudice, G. Isidori, and P. Paradisi, *J. High Energy Phys.* **04** (2012) 060.
- [22] T. Liu, in *The Future of High-Sensitivity Charm Experiments: Proceedings of the CHARM2000 Workshop, Batavia, IL, 7-9 Jun 1994* (Fermilab, Batavia, 1994), p. 375.
- [23] R. Aaij *et al.* (LHCb Collaboration), *Phys. Rev. Lett.* **108**, 111602 (2012).
- [24] D. Asner *et al.* (HFAG Collaboration), [arXiv:1010.1589](https://arxiv.org/abs/1010.1589).
- [25] Charge conjugation is implied throughout.
- [26] B. Aubert *et al.* (BABAR Collaboration), *Nucl. Instrum. Methods Phys. Res., Sect. A* **479**, 1 (2002).
- [27] K. Nakamura *et al.* (Particle Data Group), *J. Phys. G* **37**, 075021 (2010).
- [28] M. J. Oreglia, Ph.D. thesis, Report No. SLAC-R-236, 1980; J. E. Gaiser, Ph.D. thesis, Report No. SLAC-R-255, 1982; T. Skwarnicki, Ph.D. thesis, Report No. DESY F31-86-02, 1986.
- [29] S. Baker and R. D. Cousins, *Nucl. Instrum. Methods Phys. Res., Sect. A* **221**, 437 (1984).
- [30] The detector simulation is based on the GEANT 4 [31] toolkit. The simulated events are reconstructed using the same procedure as for real data.
- [31] S. Agostinelli *et al.* (GEANT4 Collaboration), *Nucl. Instrum. Methods Phys. Res., Sect. A* **506**, 250 (2003).
- [32] T. Aaltonen *et al.* (CDF Collaboration), *Phys. Rev. D* **85**, 012009 (2012).
- [33] H. N. Nelson, [arXiv:hep-ex/9908021](https://arxiv.org/abs/hep-ex/9908021).
- [34] S. Bergmann, Y. Grossman, Z. Ligeti, Y. Nir, and A. A. Petrov, *Phys. Lett. B* **486**, 418 (2000).
- [35] A. L. Kagan and M. D. Sokoloff, *Phys. Rev. D* **80**, 076008 (2009).